Computational Materials Science 112 (2016) 44–51

Contents lists available at ScienceDirect

Computational Materials Science

journal homepage: www.elsevier.com/locate/commatsci

# Validation of a novel higher-order multi-phase-field model for grain-growth simulations using anisotropic grain-boundary properties

Eisuke Miyoshi [a], Tomohiro Takaki [b,*]

[a] Department of Mechanical and System Engineering, Kyoto Institute of Technology, Matsugasaki, Sakyo, Kyoto 606-8585, Japan
[b] Faculty of Mechanical Engineering, Kyoto Institute of Technology, Matsugasaki, Sakyo, Kyoto 606-8585, Japan

ARTICLE INFO

*Article history:*
Received 13 July 2015
Received in revised form 8 October 2015
Accepted 11 October 2015
Available online 19 November 2015

*Keywords:*
Multi-phase-field model
Microstructural evolution
Grain growth
Grain boundary
Triple junction

ABSTRACT

The multi-phase-field (MPF) model proposed by Steinbach et al. has several advantages when it comes to numerically simulating the grain growth, recrystallization, and multiple phase transitions. In this study, in order to improve the accuracy of MPF simulations using the anisotropic grain-boundary energy and mobility, which depend strongly on the misorientation angles, we account for the triple-junction properties in the MPF model. Further, two-dimensional simulations of grain-boundary migrations in three-grain systems as well as simulations of abnormal grain growth in a polycrystalline system are performed using the proposed model, in order to confirm its validity. The results show that the proposed model allows for the introduction of the anisotropic energy and mobility with high accuracy for a wider range of misorientations, in contrast to the conventional model.



## 1. Introduction

When a metallic polycrystalline material is heat treated, its microstructure changes drastically through several phenomena such as multiple phase transitions, recrystallization, and grain growth [1,2]. The ability to predict and control the microstructure formed during the heat-treatment process is crucial for developing materials with desirable mechanical properties. In general, the microstructural evolution is accompanied by the migration of grain boundaries, a phenomenon that can be regarded as grain growth in a broad sense. Therefore, in order to predict the heat-treated microstructure systematically, numerical simulations based on a grain-growth model are usually performed [2].

The Monte-Carlo model [3], the cellular automaton model [4], the vertex model [5,6] and the phase-field (PF) model [7–11] are frequently used for numerically modeling grain growth [12]. The PF model can successfully simulate complicated microstructural evolutions on real-time and real-space scales. In addition, because this model takes into account the effects of the grain-boundary curvature, which affects the grain-growth behavior, the curvature does not have to be calculated. Hence, the PF model is considered the most suitable one for simulating grain growth. The following are the commonly used polycrystalline-grain-growth models within the framework of the PF model: the KWC model [13–16] proposed by Kobayashi, Warren, and Carter and the multi-phase-field (MPF) models reported by Steinbach et al. [17,18] and Chen et al. [19,20]. The KWC model can express an arbitrary number of crystal orientations using only two order parameters [21]. In addition, the coalescence of the grains, owing to their rotation, is also taken into consideration. However, the time-evolution equations of the order parameters are singular diffusion equations and thus the time increment for the numerical simulations must be kept very small. Furthermore, using this model, it is difficult to express the grain growth quantitatively while taking into account the misorientation-dependent grain-boundary energies. In contrast, the MPF model developed by Steinbach et al. [17,18] exhibits numerous advantages, in that the coefficients of the time-evolution equation are related directly to the material parameters. Thus, a quantitative evaluation of the evolution of the microstructure is possible. Moreover, it is easy to introduce the active parameter tracking algorithm [22–24] proposed by Kim et al. in this model [25]; this increases the computation speed significantly. Thus, the MPF model is more suitable as a grain-growth model, as it lowers the computational cost and allows for accurate simulations of the microstructural evolution during heat treatments [26–30].

The dependencies of the grain-boundary energy and mobility on the misorientation angle [1,31–34] have a significant effect on

* Corresponding author. Tel./fax: +81 75 724 7317.
*E-mail address:* takaki@kit.ac.jp (T. Takaki).

http://dx.doi.org/10.1016/j.commatsci.2015.10.010
0927-0256/

both the growth kinetics and the morphology of the grains [34]. Thus, it is important to take into account the misorientation-dependent properties in the MPF model. However, the MPF model developed by Steinbach et al. does not allow for the introduction of the misorientation dependencies with high accuracy. This is because the model becomes numerically unstable in the case of calculations where the energies of the grain boundaries adjoining a triple junction exhibit large differences. To overcome this issue, Garcke et al. [35,36] and Hirouchi et al. [37] proposed a modified model having a higher-order term representing the free energy of the triple junction. However, this model, which is referred to as the higher-order MPF model, exhibits a few problems. For instance, the correct way of determining the coefficient of the higher-order term has not been established. While some groups set the coefficient as a constant [35,36,38], Hirouchi et al. determined it using an assumed equation [37]. However, as discussed in Section 3, the accuracy of the higher-order model depends on the value of the coefficient. In addition, the optimum value of the coefficient varies with the conditions. Thus, it is believed that the coefficient must be modeled through minute evaluations of the accuracy. Further, the limits of the applicability of the model, that is, the range of differences in the grain-boundary energies for which the model can be used, have not been elucidated. Finally, the accuracy of the model in the case where the mobilities of the different boundaries exhibit large differences remains untested.

The purpose of this paper is to propose the appropriate values for the parameters of the higher-order MPF model and to show the accuracy as well as the limits of applicability of the model for two-dimensional cases with respect to predicting heat-treated microstructures. First, in Section 2, we suggest a higher-order MPF model based on the model reported by Steinbach et al. [17,18]. Next, the coefficient of the higher-order term is modeled in Section 3. In this section, we also determine the effects of large differences in boundary mobilities on the accuracy of the MPF model and attempt to improve the accuracy of the model by introducing a triple-junction mobility. Finally, in Section 4, through a series of grain-growth simulations based on the modeled parameters, we investigate the accuracy and the limits of applicability of the proposed higher-order model.

## 2. Higher-order multi-phase-field model

On the basis of the MPF model proposed by Steinbach et al. [17,18], we derive the time-evolution equation for the higher-order MPF model. Let us consider a polycrystalline system consisting of $N$ grains. In the MPF model, such a system is represented by the phase-field variables $\phi_\alpha$ ($\alpha = 1, 2, \ldots, N$); these take a value of 1 in the $\alpha$th grain, 0 in the other grains, and $0 < \phi_\alpha < 1$ at the grain boundaries. Here, none of the variables is independent, and each must satisfy the following condition:

$$\sum_{\alpha=1}^{N} \phi_\alpha = 1. \tag{1}$$

The free-energy functional of the system can be written as follows using $\phi_\alpha$:

$$F = \int_V \sum_{\alpha=1}^{N} \sum_{\beta=\alpha+1}^{N} \left( W_{\alpha\beta}\phi_\alpha\phi_\beta + \sum_{\chi=\beta+1}^{N} W_{\alpha\beta\chi}\phi_\alpha\phi_\beta\phi_\chi - \frac{a_{\alpha\beta}^2}{2}\nabla\phi_\alpha \cdot \nabla\phi_\beta \right) dV, \tag{2}$$

where $W_{\alpha\beta}$ and $a_{\alpha\beta}$ are the height of the energy barrier and the gradient coefficient of the boundary between the $\alpha$th and $\beta$th grains, respectively. The second term on the right-hand side in Eq. (2) is the higher-order term representing the additional free energy of the triple junctions [35–40]. The time-evolution equation of the phase field $\phi_i$ ($i = 1, 2, \ldots, n$) satisfying Eq. (1) is given by [18]

$$\frac{\partial\phi_i}{\partial t} = -\frac{2}{n}\sum_{j=1}^{n} M_{ij}^{\phi}\left(\frac{\delta F}{\delta\phi_i} - \frac{\delta F}{\delta\phi_j}\right), \tag{3}$$

for each spatial point, where $n$ is the number of nonzero phase fields at the point and $M_{ij}^{\phi}$ is the phase-field mobility of the boundary between the $i$th and $j$th grains. The functional derivative of Eq. (3) can be calculated as

$$\frac{\delta F}{\delta\phi_i} = \sum_{k=1}^{n}\left( W_{ik}\phi_k + \sum_{l=1}^{n} W_{ikl}\phi_k\phi_l + \frac{a_{ij}^2}{2}\nabla^2\phi_k \right). \tag{4}$$

Finally, the time-evolution equation reduces to

$$\frac{\partial\phi_i}{\partial t} = -\frac{2}{n}\sum_{j=1}^{n} M_{ij}^{\phi}\left[\sum_{k=1}^{n}\left\{ (W_{ik} - W_{jk})\phi_k + \sum_{l=1}^{n}(W_{ikl} - W_{jkl})\phi_k\phi_l + \frac{1}{2}\left(a_{ik}^2 - a_{jk}^2\right)\nabla^2\phi_k \right\}\right]. \tag{5}$$

$W_{ij}$, $a_{ij}$, and $M_{ij}^{\phi}$ are related to the grain-boundary thickness, $\delta$; the grain-boundary energy, $\gamma_{ij}$; and the grain-boundary mobility, $M_{ij}$ by

$$W_{ij} = \frac{4\gamma_{ij}}{\delta}, \tag{6}$$

$$a_{ij} = \frac{2}{\pi}\sqrt{2\delta\gamma_{ij}}, \tag{7}$$

$$M_{ij}^{\phi} = \frac{\pi^2}{8\delta}M_{ij}. \tag{8}$$

Note that $\delta$ can be varied for each grain boundary similar to $\gamma_{ij}$ and $M_{ij}$. In this study, however, we kept it constant to simplify the numerical calculations.

## 3. Modeling of parameters

### 3.1. Coefficient of higher-order term: $W_{ijk}$

When grain-boundary energies with large differences are introduced in the conventional MPF model, unnecessary phases (i.e., "ghost phases" [38]) leak from the triple junctions into the grain boundaries, making the behavior of the boundaries unstable. The higher-order term in the time-evolution equation (5) is employed as a penalty term to prevent the ghost phases from leaking [35–38]. However, since the coefficient of the higher-order term $W_{ijk}$ has a significant effect on the simulation results [35], $W_{ijk}$ must be set with care. Therefore, to determine the most suitable way of determining $W_{ijk}$, we examine the optimum values of $W_{ijk}$ by evaluating the accuracy of the higher-order MPF model. For this

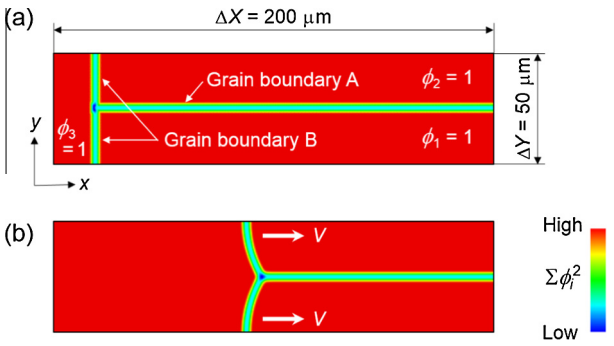


**Fig. 1.** Three-grain system used for evaluating the accuracy of the higher-order MPF model: (a) initial state and (b) steady state.

purpose, we employ the three-grain system shown in Fig. 1(a) as the simulation model; the steady-state boundary velocity, $V$, shown in Fig. 1(b), is compared with the theoretical value. The system consists of three grains represented by the phase fields $\phi_1$, $\phi_2$, and $\phi_3$. The colors in Fig. 1 represent $\sum \phi_i^2 = \phi_1^2 + \phi_2^2 + \phi_3^2$. The domain is divided by square regular lattices with a size of $\Delta x$. The domain sizes are $\Delta X = 200\,\mu m$ in the $x$-direction and $\Delta Y = 50\,\mu m$ in the $y$-direction. Zero-Neumann conditions are applied to all the sides of the system. The theoretical value of $V$, $V_{th}$, is calculated as [41,42]

$$V_{th} = M_B \frac{\gamma_A}{\Delta Y}, \tag{9}$$

where $\gamma_A$ is the energy of the grain boundary A and $M_B$ is the mobility of the grain boundary B. For each simulation run, the energy of the grain boundary B, $\gamma_B$, and the mobility of the grain boundary A, $M_A$, are fixed at $1\,J/m^2$ and $1\,m^4/(J\,s)$, respectively. On the other hand, $\gamma_A$ and $M_B$ are varied. Note that when $\gamma_A/\gamma_B \geqslant 2$ solid-state wetting [43,44] occurs, through which the grain boundary A splits into two boundaries and the triple junction disappears. Therefore, we limit $\gamma_A$ within the range $\gamma_A/\gamma_B < 2$. The time increment, $\Delta t$, is made as large as possible, so as to satisfy the stability condition of the explicit scheme.

The computational accuracy of the MPF model is dependent on the grid resolution and the grain-boundary thickness, $\delta$. Therefore, in order to determine the appropriate settings to evaluate the accuracy of the higher-order model, we first performed simulations while varying $\delta$ and the resolution, $\Delta Y/\Delta x$; this allowed us to determine the changes in the relative error $(V - V_{th})/V_{th}$. The results are shown in Fig. 2. Here, the conditions $\gamma_A = \gamma_B$ and $M_B = M_A$ were employed. It can be seen from the results that $\delta = 4\Delta x$ yields an error larger than 5% for any $\Delta Y/\Delta x$. Further, in the cases of $\delta = 8\Delta x$ and $10\Delta x$, although the errors decrease with the increase in $\Delta Y/\Delta x$, it is expected that an extremely high resolution is necessary to decrease the errors to approximately zero. In contrast, the results obtained for $\delta = 6\Delta x$ are far more accurate; the error is approximately 1% even for $\Delta Y/\Delta x = 10$ and less than 0.1% for $\Delta Y/\Delta x = 50$. Thus, to optimize the computational accuracy and cost, we used $\delta = 6\Delta x$ and $\Delta Y/\Delta x = 50$.

Next, simulations were performed under the above-described conditions for various energy ratios $\gamma_A/\gamma_B$, with $M_B = M_A$. For each $\gamma_A/\gamma_B$ value, the coefficient of the higher-order term $W_{123}$ was varied by $0.1\,MJ/m^3$, and the changes in the relative error $(V - V_{th})/V_{th}$ were determined. Here, $W_{123}$ was limited to zero or positive values. This was because setting $W_{123}$ to a negative value causes the free energy of the triple junction to become lower than those of the grain boundaries. As a result, the boundaries become

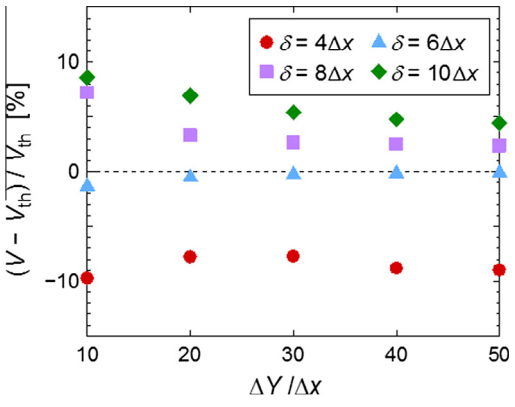


**Fig. 2.** Variations in $(V - V_{th})/V_{th}$ with $\Delta Y/\Delta x$ for the different grain-boundary thickness, $\delta$, values.

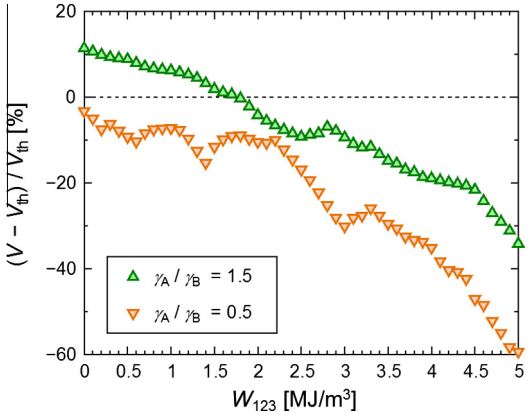


**Fig. 3.** Variations in $(V - V_{th})/V_{th}$ with $W_{123}$.

unstable. The simulation results for $\gamma_A/\gamma_B = 0.5$ and 1.5 are shown in Fig. 3. In both the cases, as $W_{123}$ increases, $(V - V_{th})/V_{th}$ decreases almost monotonically. For $\gamma_A/\gamma_B = 1.5$, the magnitude of the relative error, $|(V - V_{th})/V_{th}|$, becomes approximately zero at $W_{123} = 1.8\,MJ/m^3$. For $\gamma_A/\gamma_B = 0.5$, $|(V - V_{th})/V_{th}|$ does not become zero, reaching its minimum value at $W_{123} = 0\,MJ/m^3$. These values of $W_{123}$, which minimize $|(V - V_{th})/V_{th}|$, are considered the optimum values. The circles in Fig. 4(a) show the optimum value of $W_{123}$ for each $\gamma_A/\gamma_B$ value. Here, $W_{123}$ is normalized with respect to the average of the energy barriers, which is $W_{ave} = (W_{12} + W_{23} + W_{31})/3$. The open and closed circles in Fig. 4(b) represent the $(V - V_{th})/V_{th}$ values in the case of the conventional MPF model ($W_{123} = 0$) and the higher-order model using the optimum $W_{123}$ value in Fig. 4(a), respectively. From these results, we can conclude that, for $\gamma_A/\gamma_B > 1$, the optimum $W_{123}$ value increases monotonically and by using the optimum value, $(V - V_{th})/V_{th}$ can be made zero. For $0.5 \leqslant \gamma_A/\gamma_B \leqslant 1$, the optimum $W_{123}$ is zero for most cases, suggesting that the higher-order term does not work effectively. However, $|(V - V_{th})/V_{th}|$ remains less than 5%, and the accuracy of the model is relatively high. For $\gamma_A/\gamma_B < 0.5$, as $\gamma_A/\gamma_B$ decreases, $|(V - V_{th})/V_{th}|$ increases sharply. In this range, there is significant leakage of ghost phases into the grain boundaries for all values of $W_{123}$.

On the basis of the above-mentioned results, it can be concluded the higher-order term cannot stabilize computations for $\gamma_A/\gamma_B < 0.5$. Further, we find that $W_{ijk}$ should be determined as follows: in cases where two low-energy boundaries and one high-energy boundary intersect at a junction, the $W_{ijk}$ value for the junction should be set in accordance with the difference in the energies, as shown in Fig. 4(a). In the other cases, $W_{ijk}$ should be set to zero. Using these conditions, we can model $W_{ijk}$ as follows:

$$W_{ijk} = \begin{cases} k\left(W_{max} - \frac{W_{median} + W_{min}}{2}\right) & \text{for } 2W_{median} \leqslant W_{max} + W_{min} \\ 0 & \text{for } 2W_{median} > W_{max} + W_{min} \end{cases}, \tag{10}$$

where $W_{max}$, $W_{median}$, and $W_{min}$ are the maximum, median, and minimum energy barriers, respectively, for the grain boundaries adjoining the triple junction, and $k$ is a constant for adjusting the contribution of the higher-order term. This formula can be applied in the cases where the three boundaries have different energies. The curves for Eq. (10) for $k = 3$, 4, 5, and 6 are shown in Fig. 4(a) as solid lines; it can be seen that $k = 5$ corresponds to the optimum $W_{ijk}$ value obtained from the simulations. Next, using these values of $k$, we evaluated the accuracy of the higher-order model using Eq. (10) in the same manner as that described above. The results are shown in Fig. 4(b). The results for $\gamma_A/\gamma_B \leqslant 1$ are omitted because

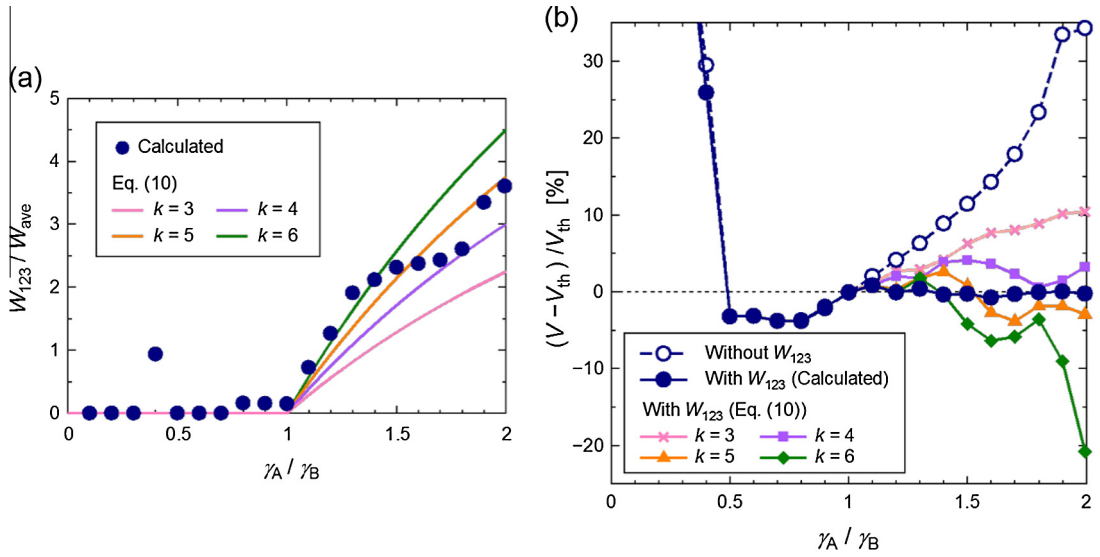


**Fig. 4.** Variations in the (a) optimum value of $W_{123}$ for minimizing $|(V - V_{th})/V_{th}|$ and (b) $(V - V_{th})/V_{th}$ with and without the higher-order term for different $\gamma_A/\gamma_B$ values, as calculated using the model shown in Fig. 1.

$W_{ijk} = 0$ in this range. As shown in Fig. 4(b), the error decreases drastically with an increase in $k$. However, for $k \geqslant 5$, the error increases again on the negative side. When the error becomes negative, the triple-junction region with $n = 3$ shrinks markedly, and the behavior becomes unstable, especially when the misorientation dependencies of the grain-boundary energy and mobility are taken into account simultaneously. Therefore, in the simulations that follow, we employed $k = 4$ with a small positive error for all $\gamma_A/\gamma_B$.

### 3.2. Triple-junction mobility: $M_{ijk}$

Guo and Steinbach [45] performed an MPF simulation while setting the mobilities of the grain boundaries around a triple junction to 2:3:4 and concluded that the differences in the mobilities do not have significant effects on simulation accuracy. However, for cases with wider-ranging mobilities, the accuracy of the MPF model has not been tested. Therefore, to elucidate the accuracy of the model, we performed simulations using the system shown in Fig. 1 and determined the relative error $(V - V_{th})/V_{th}$ for various $M_B/M_A$ values. Here, the $\gamma_A/\gamma_B$ value was set to 1. Fig. 5 shows the relationships between $(V - V_{th})/V_{th}$ and $M_B/M_A$. The circles in the figure represent the simulation results. For $M_B/M_A > 1$, although $V$ is a little larger than the theoretical value, $V_{th}$, the error is not more than 10%. On the other hand, for $M_B/M_A > 1$, $V$ becomes significantly smaller than $V_{th}$ with a decrease in $M_B/M_A$, and the error is approximately 80% for $M_B/M_A = 0.01$. These results indicate that when the differences in the mobilities are large, they have a marked effect on the accuracy of the MPF model. This can be attributed to the manner in which the phase-field mobility, $M_{ij}^{\phi}$, is defined. When $M_{ij}^{\phi}$ as defined by Eq. (8) is substituted in the time-evolution equation (5), the migration of the triple junction, $ijk$, is determined by the linear superposition of the grain-boundary mobilities, $M_{ij}$, $M_{jk}$, and $M_{ki}$. For this reason, when one of the mobilities in the triple junction much higher or lower than the others, it has a significant effect on the migration of the junction. Therefore, we modify the definition of $M_{ij}^{\phi}$ in triple junctions as follows:

$$\left.\begin{aligned} M_{ij}^{\phi} = M_{jk}^{\phi} = M_{ki}^{\phi} = \tfrac{\pi^2}{8\delta} M_{ijk} \\ M_{ijk} = M_{ij}\omega_{ij} + M_{jk}\omega_{jk} + M_{ki}\omega_{ki} \end{aligned}\right\} \text{ only for } n = 3, \tag{11}$$

where $M_{ijk}$ is the triple-junction mobility and $\omega_{ij}$ is the weight function defined as follows using the average of the grain-boundary mobilities $M_{ave} = (M_{ij} + M_{jk} + M_{ki})/3$:

$$\omega_{ij} = \frac{1}{2}\left(1 - \frac{|M_{ij} - M_{ave}|^m}{|M_{ij} - M_{ave}|^m + |M_{jk} - M_{ave}|^m + |M_{ki} - M_{ave}|^m}\right), \tag{12}$$

where the exponent $m$ is the arbitrary constant representing the strength of the weighting. When $m = 0$, $M_{ijk} = M_{ave}$. To test the effects of this modification, we evaluated the accuracy of the MPF model using Eq. (11) in the same manner as that described above. The crosses, squares, triangles, and diamonds in Fig. 5 represent the results obtained for $m = 0$, 5, 10, and 15, respectively. From these results, it is confirmed that the magnitude of the error was less than approximately 10% over $0.01 \leqslant M_B/M_A \leqslant 100$. In particular, for $m \geqslant 10$ the results almost converge to zero. Therefore, for the rest of the study, we used $m = 10$.

It should be noted that an alternative way of determining the weight function, $\omega_{ij}$, has been proposed by Folch and Plapp [46], who expressed $\omega_{ij}$ as a function of the phase fields. Using this method, the higher-order model proposed in Ref. [37] expresses $\omega_{ij}$ as $\phi_i\phi_j/(\phi_i\phi_j + \phi_j\phi_k + \phi_k\phi_i)$. However, when this expression is

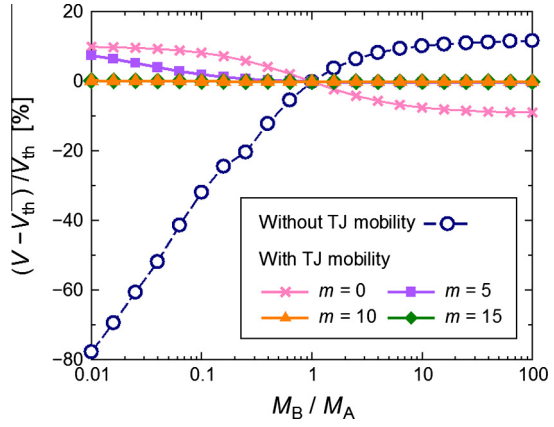


**Fig. 5.** Variations in $(V - V_{th})/V_{th}$ with $M_B/M_A$ as calculated using the model in Fig. 1 for $\gamma_A/\gamma_B = 1$.

employed, if the grain-boundary mobility at a junction is very small, an artificial junction drag occurs on the boundaries. For example, in the extreme case where the mobility of the boundary A ($M_A$) (see Fig. 1) equals zero, boundary B does not migrate for any value of the mobility, $M_B$. In contrast, even for such cases, $\omega_{ij}$ when defined as Eq. (12) yields a result almost consistent with the theoretical one and thus can be considered more versatile.

## 4. Validations of the novel higher-order MPF model

We validate the proposed higher-order MPF model using Eq. (10) with $k = 4$ and Eq. (11) with $m = 10$. First, the accuracy of the model is determined with simple three-grain systems. Here, the misorientation-dependent grain-boundary energy and mobility are introduced. Next, abnormal-grain-growth simulations are performed in polycrystalline systems using nonuniform grain-boundary properties.

### 4.1. Grain-boundary migrations in three-grain systems

We examine the accuracy of the higher-order model from the viewpoints of the dynamics and statics of grain boundaries. In this case too, we use the system shown in Fig. 1 for the dynamics-based evaluation of the grain boundaries. In addition, the system shown in Fig. 6(a) is employed for evaluating the equilibrium junction angle, $\alpha$, which is shown in Fig. 6(b). As was the case with the system in Fig. 1, that in Fig. 6 also consists of three grains, which are represented by the phase fields $\phi_1$, $\phi_2$, and $\phi_3$. The domain is divided by regular square lattices with a size of $\Delta x = 1$ μm. The domain size in the $y$-direction, $\Delta Y$, is fixed at $100\Delta x$, while that in the $x$-direction, $\Delta X$, is varied, so that the triple junction does not move out of the domain. Zero-Neumann conditions are applied to the left and right sides of the system, and continuous-gradient conditions [45] to the top and bottom sides. The grain-boundary thickness, $\delta$, is $6\Delta x$. The theoretical value of $\alpha$, $\alpha_{th}$, can be calculated as follows using Young's law [31]:

$$\alpha_{th} = 2\cos^{-1}\left(\frac{\gamma_B}{2\gamma_A}\right). \tag{13}$$

For the models in both Figs. 1 and 6, the misorientation ($\Delta\theta$) dependency of the grain-boundary energy, $\gamma$, is introduced using the well-known Read–Shockley (RS) model [47]:

$$\gamma = \begin{cases} \gamma_m \frac{\Delta\theta}{\Delta\theta_m}\left\{1 - \ln\left(\frac{\Delta\theta}{\Delta\theta_m}\right)\right\} & \text{for } \Delta\theta < \Delta\theta_m \\ \gamma_m & \text{for } \Delta\theta \geqslant \Delta\theta_m \end{cases}, \tag{14}$$

where $\gamma_m = 1\ \mathrm{J/m^2}$ and $\Delta\theta_m = 15°$ are the energy and minimum misorientation of the high-angle grain boundaries, respectively. The misorientation-dependent grain-boundary mobility $M$ is also introduced using the model proposed by Humphreys [48]:

$$M = \begin{cases} M_m\left[1 - \exp\left\{-5\left(\frac{\Delta\theta}{\Delta\theta_m}\right)^4\right\}\right] & \text{for } \Delta\theta < \Delta\theta_m \\ M_m & \text{for } \Delta\theta \geqslant \Delta\theta_m \end{cases}, \tag{15}$$

where $M_m = 1\ \mathrm{m^4/(J\,s)}$ is the mobility of the high-angle grain boundaries.

During each simulation run, the misorientation of the boundary A, $\Delta\theta_A$, and that of the boundary B, $\Delta\theta_B$, are varied up to $\Delta\theta_m = 15°$. Here, either $\Delta\theta_A$ or $\Delta\theta_B$ is fixed to $\Delta\theta_m$, while the other is varied. Note that $\Delta\theta_B$ must be limited within the range $\Delta\theta_B \geqslant 3°$, in order to prevent solid-state wetting [43,44]. The time increment, $\Delta t$, is made as large as possible, so as to satisfy the stability condition of the explicit scheme.

Simulations were performed under the above-described conditions for various $\Delta\theta$ values using the conventional and higher-order MPF models, and the $V$ and $\alpha$ values were calculated and compared with their theoretical counterparts. Fig. 7 shows the variations in the relative errors $(V - V_{th})/V_{th}$ and $(\alpha - \alpha_{th})/\alpha_{th}$ with $\theta_A$, while Fig. 8 shows the variations in the errors with $\Delta\theta_B$. In Fig. 7(a), as $\Delta\theta_A$ decreases, $(V - V_{th})/V_{th}$ as determined using the conventional model increases monotonically. The magnitude of the error remains less than 10% in the range $\Delta\theta_A \geqslant 6°$, but increases sharply for $\Delta\theta_A \leqslant 5°$ and reaches 100% at $\Delta\theta_A = 2°$. On the other hand, although $(V - V_{th})/V_{th}$ as determined using the higher-order model decreases till $\Delta\theta_A = 3°$, the magnitude is less than 5%. For $\Delta\theta_A \leqslant 2°$, $(V - V_{th})/V_{th}$ increases discontinuously, becoming approximately 60% at $\Delta\theta_A = 1°$. As can be seen from Fig. 7(b), $(\alpha - \alpha_{th})/\alpha_{th}$ as determined using both models is within ±5%. In particular, the error determined using the higher-order model is, at most, 2%, and the accuracy is notably high. Further, as can be seen from Fig. 8(a), as $\Delta\theta_B$ decreases, $(V - V_{th})/V_{th}$ as determined by the conventional model decreases, while that determined using the higher-order model increases monotonically. However, while the conventional model results in an error greater than 30% at $\Delta\theta_B = 3°$, the higher-order model yields an error lower than 5%. As can be seen from Fig. 8(b), $(\alpha - \alpha_{th})/\alpha_{th}$ as determined using the conventional model increases with a decrease in $\Delta\theta_B$ and becomes 60% at $\Delta\theta_B = 4°$. When $\Delta\theta_B$ is decreased further, it becomes impossible to calculate $\alpha$, owing to the splitting of the grain boundary A. In contrast, the higher-order model yields results almost consistent with the theory for $\Delta\theta_B \geqslant 5°$. Further, $(V - V_{th})/V_{th}$ increases for $\Delta\theta_B \leqslant 4°$ but is approximately 10% even at $\Delta\theta_B = 3°$.

The above-described results confirm that the higher-order model allows the misorientation-dependent grain-boundary properties to be introduced with greater accuracy than does the conventional model. In particular, for $\Delta\theta \geqslant 3°$, the magnitude of the error remains less than approximately 10%. However, the only drawback of the higher-order model is that there is no increase in the accuracy of the $V$ values for $\Delta\theta_A \leqslant 2°$. In this range, the energy ratio $\gamma_A/\gamma_B$ is lower than 0.5, and a significant degree of leakage of ghost phases continues to occur, as described in Section 3.1. When simulating polycrystalline grain growth in a more general manner using the higher-order model, the anisotropic properties should be introduced within the range for which the ratio of the maximum and minimum boundary energies is 2 or lower; this corresponds to $\Delta\theta \geqslant 3°$ in the RS model. Whether this range is enough or not depends on the purpose of the simulation. However, for predicting heat-treated microstructures, the range is probably enough for the following reason: on the basis of observations of heat-treated microstructures performed using scanning electron microscopy and transmission electron microscopy, it has been confirmed that low-angle boundaries with misorientation angles lower than approximately 2° are swept up rapidly; this is probably owing to mechanisms other than grain-boundary migrations [49,50]. Therefore, such low-angle boundaries are considered to have little effect on the grain-growth behavior.

### 4.2. Growth of abnormal grains in polycrystalline systems

In textured systems, anisotropic grain-boundary properties can cause a few grains to undergo abnormal growth [48,51–53]. This abnormal growth leads to rapid grain coarsening and the development of a texture. Moreover, the abnormal growth of subgrains is considered to be one of the reasons for recrystallization. A few research groups [41,54–58] performed curvature-driven subgrain-growth simulations while taking the anisotropy of the properties into account and observed the nucleation of the recrystallized grains through abnormal subgrain growth. Hence, abnormal grain growth is believed to be one of the most important

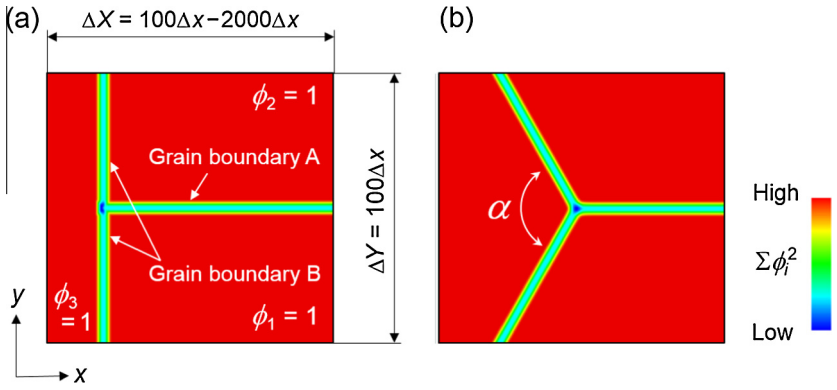


**Fig. 6.** Three-grain system used for the statics-based evaluation of the grain boundaries with misorientation-dependent properties: (a) initial state and (b) equilibrium state.

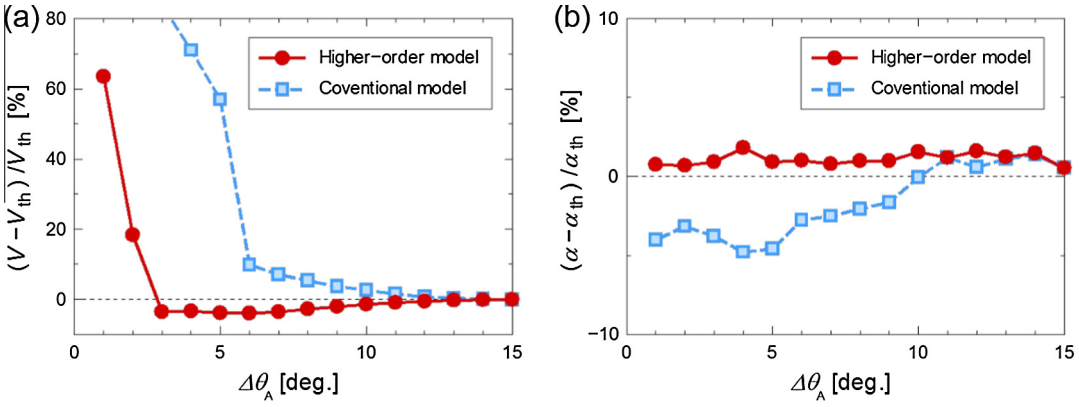


**Fig. 7.** Variations in (a) $(V - V_{th})/V_{th}$ and (b) $(\alpha - \alpha_{th})/\alpha_{th}$ with $\Delta\theta_A$, as calculated using the models shown in Figs. 1 and 6, where $\Delta\theta_B$ is fixed at 15°.

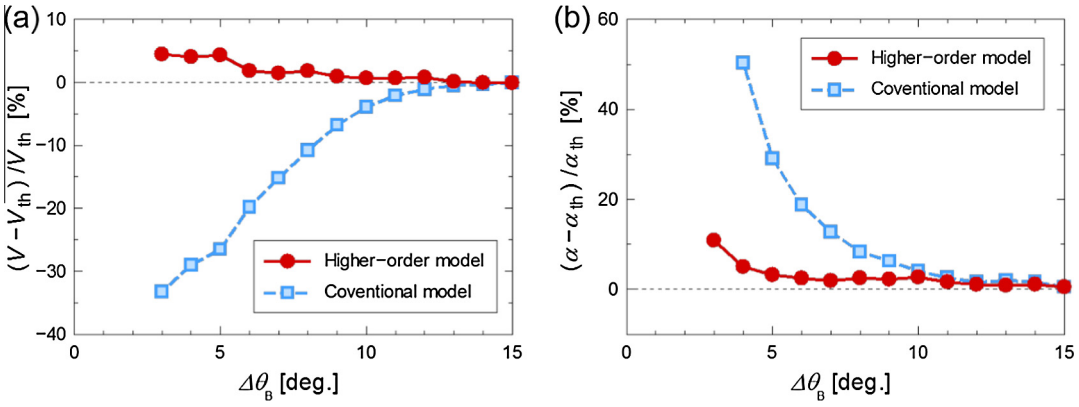


**Fig. 8.** Variations in (a) $(V - V_{th})/V_{th}$ and (b) $(\alpha - \alpha_{th})/\alpha_{th}$ with $\Delta\theta_B$, as calculated using the models shown in Figs. 1 and 6, where $\Delta\theta_A$ is fixed at 15°.

phenomena related to the anisotropic grain-boundary properties. Therefore, to test the accuracy of the novel higher-order MPF model while taking into account the properties, we performed a series of simulations on the growth of abnormal grains in grain assemblies. For this purpose, a polycrystalline system [59], shown in Fig. 9(a), was employed as the simulation model. Here, a recrystallized grain abnormally grows and encroaches on the subgrains; the steady-state velocity of the recrystallized-grain boundary, $V_R$, is used as the benchmark of the simulation accuracy. The domain is divided into a grid of 1000 × 1000 by square regular lattices with a size of $\Delta x = 0.05$ μm. The recrystallized grain with a straight-line boundary is placed in the left-hand region of the domain. The rest of the domain is filled with a number of subgrains with a mean diameter $D_{ave} = 1.25$ μm. The initial subgrain structure is created as follows: first, the positions of the nuclei are assigned using random numbers. Next, the arranged nuclei are grown through a normal grain-growth simulation. As a result, the subgrains have random shapes. Zero-Neumann conditions are applied to the left and right sides of the system and periodic conditions to the top and bottom sides. The grain boundary thickness, $\delta$, is $6\Delta x = 0.3$ μm.

For each simulation run, the energies of the grain boundaries between the subgrains, $\gamma_S$, are set to a constant value of 0.25 J/m$^2$. On the other hand, the boundary energy of the recrystallized grain, $\gamma_R$, is varied within the range $0.5 \leqslant \gamma_S/\gamma_R < 2.0$. In this range, solid-state wetting does not occur, and the applicability limit of the

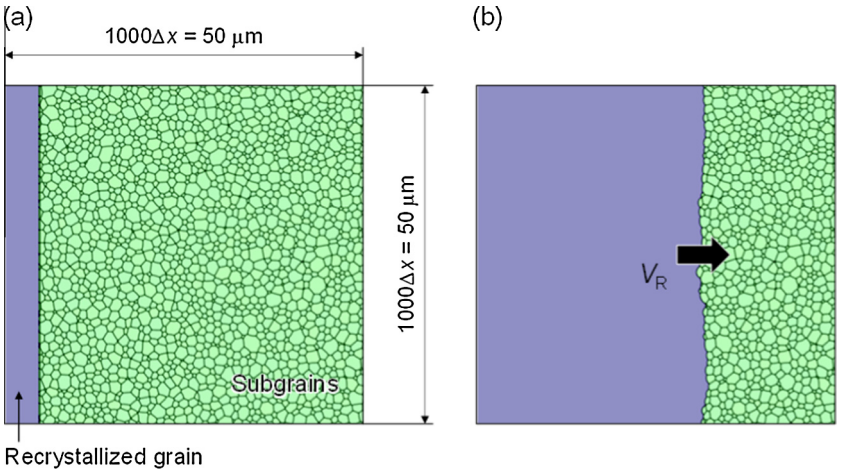


**Fig. 9.** Polycrystalline system used for the simulation of abnormal grain growth: (a) initial state and (b) steady state after 200,000 steps for $\gamma_R = \gamma_S$. The initial structure is created through a normal grain-growth simulation.

MPF model mentioned in the previous section is not exceeded. The mobilities of the grain boundaries between the subgrains are all set to zero, and a nonzero mobility $M_R = 5.0 \times 10^{-13}$ m$^4$/(J s) is used only for the recrystallized-grain boundary. Using the above-mentioned settings, the growth of recrystallized grains under constant driving forces is modeled while ignoring the recovery in the subgrain structure. The time increment is set to $5.0 \times 10^{-4}$ s. Fig. 9(b) exhibits the simulation result, which shows the polycrystalline morphology after 200,000 steps for $\gamma_R = \gamma_S$. It can be seen that the recrystallized-grain boundary migrates while maintaining the approximately straight-line configuration. The temporal variation in $V_R$ during the same simulation is shown in Fig. 10; $V_R$ fluctuates within ±10% but can be considered as being constant on the whole.

In the simulations performed under the conditions mentioned above, $V_R$ is calculated for various $\gamma_R$ values. Here, $V_R$ is obtained by averaging the velocities from 5000 steps to the time when the recrystallized-grain boundary reaches the right side of the domain. In addition, five simulations are performed for different initial structures for every $\gamma_S/\gamma_R$, in order to elucidate the effects of the initial structure. Fig. 11 shows the relationships between $V_R$ and the energy ratio $\gamma_S/\gamma_R$ obtained using the conventional and higher-order MPF models. At $\gamma_S/\gamma_R = 1$, $V_R$ as determined using the conventional model is 0.133 μm/s, while that obtained using the higher-order model is 0.132 μm/s; these values are almost similar. Because the driving force for the growth of the recrystallized grains depends only on the properties of the subgrains [48], it is expected that $V_R$ will remain constant for all $\gamma_R$. However, for $\gamma_S/\gamma_R < 1$, the calculated value of $V_R$ is larger than that at $\gamma_S/\gamma_R = 1$; this is true for both models. The deviations between $V_R$ at $\gamma_S/\gamma_R = 0.5$ and that at $\gamma_S/\gamma_R = 1$ are approximately 9% and 6%, respectively, in the case of the conventional and higher-order models. The higher-order model is slightly more accurate than the conventional model. For $\gamma_S/\gamma_R > 1$, $V_R$, as determined using the conventional model, increases sharply with an increase in $\gamma_S/\gamma_R$. On the other hand, the higher-order model yields a deviation that is less than 10% and is thus much more accurate than the conventional model. The range $\gamma_S/\gamma_R > 1$ corresponds to the case where the recrystallized-grain boundary is a coincident site lattice (CSL) boundary with a low energy and high mobility. During actual heat-treatment processes, it is often observed that the grains surrounded by such CSL boundaries, for example, Σ7 boundaries with misorientations of approximately 40° around the ⟨1 1 1⟩ axis, grow abnormally [1,31]. Thus, the behavior of CSL boundaries is believed to be important with respect to abnormal grain growth. On the basis of these points, the higher-order model can be considered more advantageous than the conventional one for simulating abnormal grain growth.

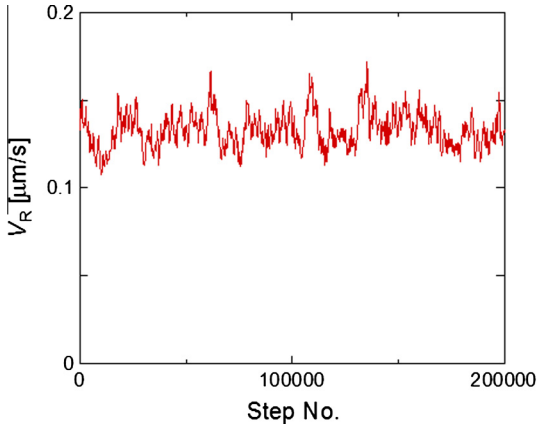


**Fig. 10.** Temporal evolutions of $V_R$ as calculated using the model in Fig. 9 for $\gamma_R = \gamma_S$.

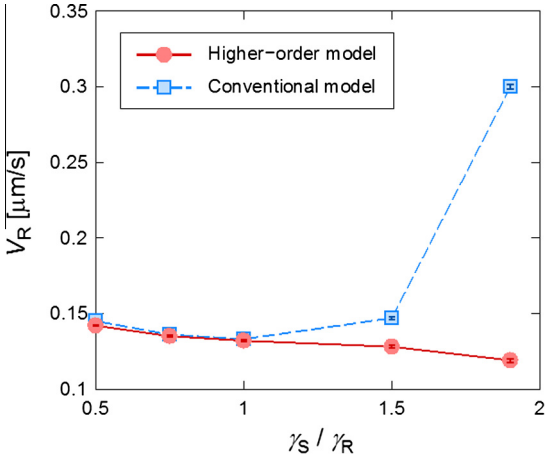


**Fig. 11.** Variations in $V_R$ with $\gamma_S/\gamma_R$ as calculated using the model in Fig. 9.

## 5. Conclusions

In this study, in order to improve the accuracy of MPF grain-growth simulations by introducing a higher-order term, we proposed a novel method for determining the values of the simulation parameters and validated the accuracy of the method. First, grain-growth simulations were performed using a three-grain system containing a triple junction, and the accuracy of the higher-order MPF model was evaluated. Based on the obtained results, the appropriate model for the coefficient of the higher-order term was examined. Next, using the higher-order model with the modeled parameters, grain-boundary migrations in the three-grain system and abnormal grain growth in a polycrystalline system were simulated while taking into account the misorientation dependencies of the grain-boundary properties. Further, on the basis of the obtained results, the accuracy and applicability limits of the higher-order model were discussed while taking the predictions related to the heat-treated microstructure into consideration. The results can be summarized as follows:

(1) In the cases where low-energy grain boundaries migrate toward a high-energy boundary, by setting the coefficient of the higher-order term to the appropriate value, the simulation accuracy of the higher-order MPF model could be improved significantly. On the other hand, in the cases where high-energy grain boundaries migrate toward a low-energy boundary, the accuracy could not be improved. If the accuracy needs to be improved under such conditions, the model must be modified in ways other than that involving the introduction of a higher-order term.
(2) On varying the mobilities of each grain boundary around a triple junction, the accuracy of the MPF model decreased significantly. However, this problem could be resolved almost completely by introducing the mobility of the triple junction proposed in this study.
(3) When the misorientation dependencies of the grain-boundary properties were introduced using the RS model and that proposed by Humphreys, the higher-order model resulted in stable computations for misorientation angles as low as 3°. This range is believed to be suitable for simulating grain growth during heat treatment.
(4) Through the abnormal-grain-growth simulations performed using the boundary energies in the grain assembly as the driving force, it was confirmed that the higher-order model can simulate the behavior of CSL boundaries with a low energy and high mobility accurately. This is important for simulating abnormal grain growth.

As the first step in developing an accurate grain-growth model, this study focused on two-dimensional simulations for idealized grain structures. Such simulations can be expected to determine the grain-boundary properties by comparing the results to those of quasi-two-dimensional molecular-dynamics simulations [60,61]. However, three-dimensional simulations are essential for simulating actual grain growth [25]. Therefore, as the next step, we plan to test the applicability of the present model for simulating three-dimensional grain growth. Further, because quadruple junctions might have a significant effect on three-dimensional grain growth [31], modifying the model such that it takes into account such higher-order junctions is also important. We believe that the present method, in which the properties of triple junctions are accounted for, can be extended to take into consideration the properties of higher-order junctions as well.

## References

[1] F.J. Humphreys, M. Hatherly, Recrystallization and Related Annealing Phenomena, second ed., Pergamon Press, Oxford, 2004.
[2] D. Raabe, F. Roters, F. Barlat, L.-Q. Chen, Continuum Scale Simulation of Engineering Materials, Wiley-VCH, Weinheim, 2004.
[3] D.J. Srolovitz, G.S. Grest, M.P. Anderson, Acta Metall. 34 (1986) 1833–1845.
[4] H.W. Hesselbarth, I.R. Göbel, Acta Metall. Mater. 39 (1991) 2135–2143.
[5] K. Piękoś, J. Tarasiuk, K. Wierzbanowski, B. Bacroix, Comput. Mater. Sci. 42 (2008) 584–594.
[6] D. Weygand, Y. Brechett, J. Lépinoux, Philos. Mag. B 80 (2009) 1987–1996.
[7] T. Takaki, ISIJ Int. 54 (2014) 437–444.
[8] Y. Wang, J. Li, Acta Mater. 58 (2010) 1212–1235.
[9] I. Steinbach, Model. Simul. Mater. Sci. Eng. 17 (2009) 073001.
[10] T. Takaki, A. Yamanaka, Y. Tomita, Adv. Struct. Mat. 64 (2015) 441–459.
[11] L.-Q. Chen, Annu. Rev. Mater. Res. 32 (2002) 113–140.
[12] M. Miodownik, J. Light Met. 2 (2002) 125–135.
[13] R. Kobayashi, J.A. Warren, W.C. Carter, Physica D 119 (1998) 415–423.
[14] J.A. Warren, W.C. Carter, R. Kobayashi, Physica A 261 (1998) 159–166.
[15] R. Kobayashi, J.A. Warren, W.C. Carter, Physica D 140 (2000) 141–150.
[16] J.A. Warren, R. Kobayashi, A.E. Lobkovsky, W.C. Carter, Acta Mater. 51 (2003) 6035–6058.
[17] I. Steinbach, F. Pezzolla, B. Nestler, M. Seeßelberg, R. Prieler, G.J. Schmitz, J.L.L. Rezende, Physica D 94 (1996) 135–147.
[18] I. Steinbach, F. Pezzolla, Physica D 134 (1999) 385–393.
[19] L.-Q. Chen, W. Yang, Phys. Rev. B 50 (1994) 15752–15756.
[20] D. Fan, L.-Q. Chen, Acta Mater. 45 (1997) 611–622.
[21] T. Takaki, K. Nakagawa, Y. Morita, E. Nakamachi, Mech. Eng. J. 2 (2015) 15–00063.
[22] T. Takaki, T. Hirouchi, Y. Hisakuni, A. Yamanaka, Y. Tomita, Mater. Trans. 49 (2008) 2559–2565.
[23] Y. Suwa, Y. Saito, H. Onodera, Comput. Mater. Sci. 44 (2008) 286–295.
[24] M. Ohno, S. Tsuchiya, K. Matsuura, Acta Mater. 59 (2011) 5700–5709.
[25] S.G. Kim, D.I. Kim, W.T. Kim, Y.B. Park, Phys. Rev. E 74 (2006) 061605.
[26] T. Takaki, Y. Hisakuni, T. Hirouchi, A. Yamanaka, Y. Tomita, Comput. Mater. Sci. 45 (2009) 881–888.
[27] A. Yamanaka, T. Takaki, T. Aoki, T. Shimokawabe, J. Comput. Sci. Technol. 6 (2012) 182–197.
[28] T. Takaki, A. Yamanaka, Y. Tomita, ISIJ Int. 51 (2011) 1717–1723.
[29] T. Takaki, C. Yoshimoto, A. Yamanaka, Y. Tomita, Int. J. Plast 52 (2014) 105–116.
[30] C. Yoshimoto, T. Takaki, ISIJ Int. 54 (2014) 452–459.
[31] G. Gottstein, L.S. Shvindlerman, Grain Boundary Migration in Metals: Thermodynamics, Kinetics, Applications, CRC Press, Boca Raton, 1999.
[32] Y. Shibuta, S. Takamoto, T. Suzuki, ISIJ Int. 48 (2008) 1582–1591.
[33] Y. Shibuta, S. Takamoto, T. Suzuki, Comput. Mater. Sci. 44 (2009) 1025–1029.
[34] M. Upmanyu, G.N. Hassold, a. Kazaryan, E.a. Holm, Y. Wang, B. Patton, D.J. Srolovitz, Interface Sci. 10 (2002) 201–216.
[35] H. Garcke, B. Nestler, B. Stoth, SIAM J. Appl. Math. 60 (1999) 295–315.
[36] B. Nestler, H. Garcke, B. Stinner, Phys. Rev. E 71 (2005) 041609.
[37] T. Hirouchi, T. Tsuru, Y. Shibutani, Comput. Mater. Sci. 53 (2012) 474–482.
[38] N. Moelans, F. Wendler, B. Nestler, Comput. Mater. Sci. 46 (2009) 479–490.
[39] M. Ohno, K. Matsuura, Acta Mater. 58 (2010) 6134–6141.
[40] T. Takaki, T. Hirouchi, Y. Tomita, J. Cryst. Growth 310 (2008) 2248–2253.
[41] E.A. Holm, M.A. Miodownik, A.D. Rollett, Acta Mater. 51 (2003) 2701–2716.
[42] E. Brosh, R. Shneck, J. Am. Ceram. Soc. 43 (2004) 640–643.
[43] H. Park, J. Appl. Phys. 95 (2004) 5515–5521.
[44] K. Ko, P. Cha, D. Spolovitz, N. Hwang, Acta Mater. 57 (2009) 838–845.
[45] W. Guo, I. Steinbach, Int. J. Mater. Res. 101 (2010) 480–485.
[46] R. Folch, M. Plapp, Phys. Rev. E 72 (2005) 011602.
[47] W.T. Read, W. Shockley, Phys. Rev. 78 (1950) 275–289.
[48] F.J. Humphreys, Acta Mater. 45 (1997) 4231.
[49] N. Kamikawa, N. Tsuji, X. Huang, N. Hansen, Acta Mater. 54 (2006) 3055–3066.
[50] T. Hirouchi, Y. Shibutani, Mater. Trans. 54 (2013) 1884–1893.
[51] A.D. Rollett, Scr. Mater. 36 (1997) 975–980.
[52] A.D. Rollett, JOM 56 (2004) 63–68.
[53] S. Wang, E.A. Holm, J. Suni, M.H. Alvi, P.N. Kalu, A.D. Rollett, Acta Mater. 59 (2011) 3872–3882.
[54] F. Han, B. Tang, H. Kou, L. Cheng, J. Li, Y. Feng, J. Mater. Sci. 49 (2014) 3253–3267.
[55] B. Radhakrishnan, G. Sarma, H. Weiland, P. Baggethun, Model. Simul. Mater. Sci. Eng. 8 (2000) 737–750.
[56] B. Radhakrishnan, G. Sarma, Philos. Mag. 84 (2004) 2341–2366.
[57] B. Radhakrishnan, G. Sarma, JOM 56 (2004) 55–62.
[58] T. Takaki, Y. Tomita, Int. J. Mech. Sci. 52 (2010) 320–328.
[59] Y. Suwa, Y. Saito, H. Onodera, Mater. Sci. Eng., A 457 (2007) 132–138.
[60] Y. Shibuta, M. Ohno, T. Takaki, JOM 67 (2015) 1793–1804.
[61] Y. Shibuta, K. Oguchi, T. Takaki, M. Ohno, Sci. Rep. 5 (2015) 13534.